DOI: 10.1002/cplu.201500104

Rational Design and Synthesis of a Highly Porous Copper-Based Interpenetrated Metal–Organic Framework for High CO_2 and H_2 Adsorption

Purnandhu Bose,[a, c] Linyi Bai,[a, c] Rakhesh Ganguly,[a] Ruqiang Zou,*[b, c] and Yanli Zhao*[a, c, d]

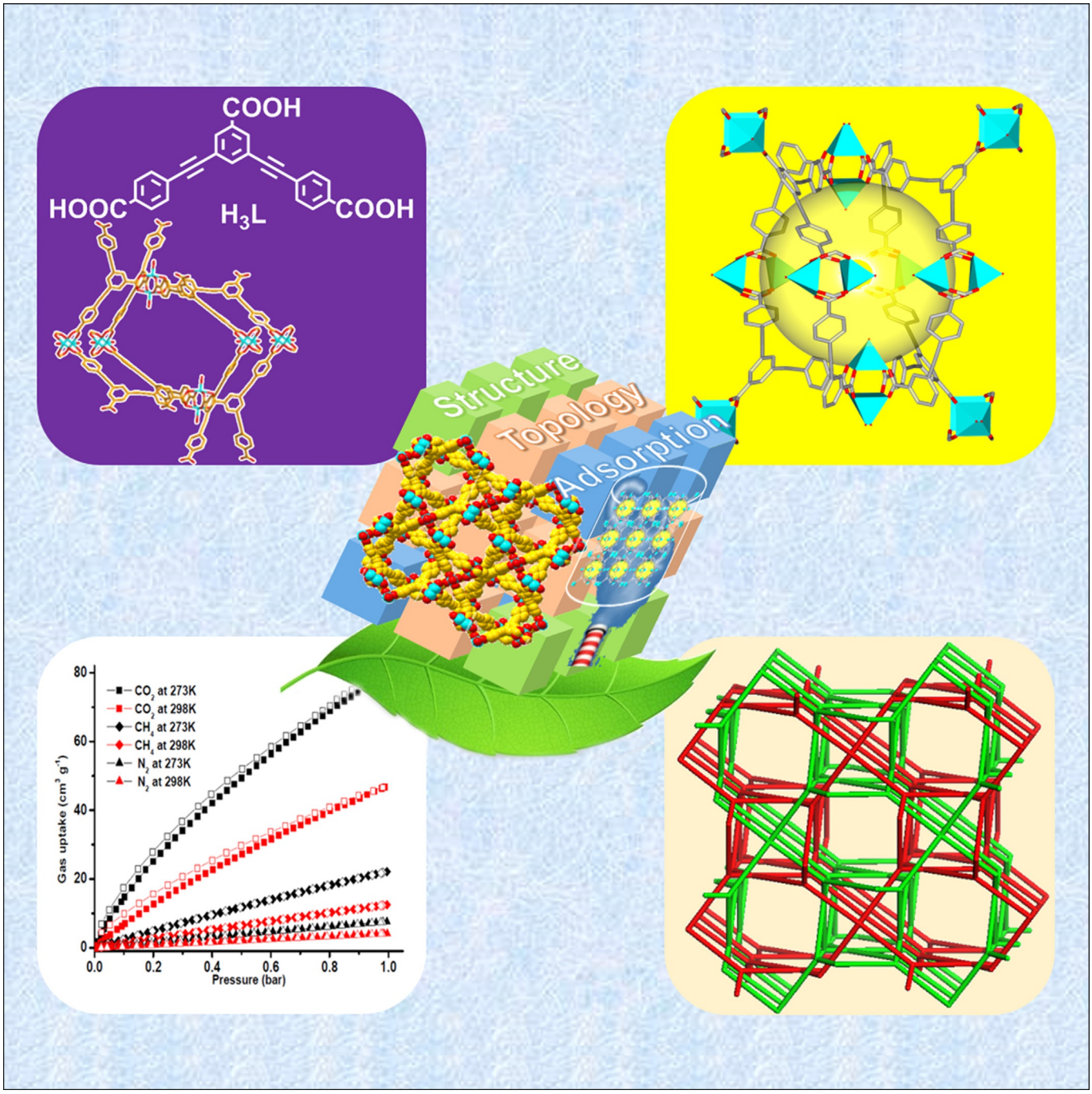

Interpenetrated metal–organic frameworks (MOFs) are often observed to show lower porosity than their non-interpenetrating analogues. It would be highly desirable if the interpenetrated MOFs could still provide high stability, high rigidity, and optimal pore size for applications. In this work, an asymmetrical tricarboxylate organic linker was rationally designed for the construction of a copper(II)-based microporous MOF with a twofold interpenetrated structure of Pt_3O_4 topology. In spite of having structural interpenetration, the activated MOF shows high porosity with a Brunauer–Emmett–Teller surface area of 2297 $m^2 g^{-1}$, and high CO_2 (15.7 wt% at 273 K and 1 bar) and H_2 uptake (1.64 wt% at 77 K and 1 bar).

Introduction

The development of novel organic–inorganic hybrid materials, specifically metal–organic frameworks (MOFs), is very promising research fields on account of their diversity and a wide range of applications. There are certain advantages that make MOFs unique, including high porosity, tunable pore size, high surface area, and diverse topologies. As a matter of fact, they have been utilized in many fields for practical applications such as gas storage and separation,[1] catalysis,[2] magnetism,[3] and molecular sensing.[4]

The rational design of organic linkers and choice of inorganic components are of great importance in order to obtain suitable MOF materials for practical applications.[5] For most of the reported cases, coordinatively unsaturated metal sites have been generated by the removal of coordinated solvent molecules for better interactions with adsorbed gas molecules. On the other hand, the porous nature of MOFs can be altered by changing the dimension of the organic linkers. Generally, larger organic linkers lead to more porous structures. However, there are certain limitations to the enlargement of the size of the organic linkers. For example, the elongation of organic linkers often results in interpenetrated networks. Obviously, the interpenetration decreases the porosity of MOFs relative to that of non-interpenetrating networks. Thus, it would be highly desirable if the interpenetrated MOFs could still present high stability, high rigidity, and optimal pore size for significant gas uptake.

[a] Dr. P. Bose, L. Bai, Dr. R. Ganguly, Prof. Dr. Y. Zhao
Division of Chemistry and Biological Chemistry
School of Physical and Mathematical Sciences
Nanyang Technological University
21 Nanyang Link, Singapore 637371 (Singapore)
E-mail: zhaoyanli@ntu.edu.sg

[b] Prof. Dr. R. Zou
Department of Materials Science and Engineering
College of Engineering, Peking University
Beijing 100871 (P. R. China)
E-mail: rzou@pku.edu.cn

[c] Dr. P. Bose, L. Bai, Prof. Dr. R. Zou, Prof. Dr. Y. Zhao
Singapore Peking University Research Centre
for a Sustainable Low-Carbon Future
1 Create Way, Singapore 138602 (Singapore)

[d] Prof. Dr. Y. Zhao
School of Materials Science and Engineering
Nanyang Technological University
50 Nanyang Avenue, Singapore 639798 (Singapore)

Supporting information for this article is available on the WWW under http://dx.doi.org/10.1002/cplu.201500104.

Part of a Special Issue to celebrate Singapore's Golden Jubilee. To view the complete issue, visit: http://dx.doi.org/10.1002/cplu.v80.8.

Highly symmetrical aromatic tricarboxylates, that is, 1,3,5-benzenetricarboxylic acid[5,6] and its derivative 1,3,5-benzenetrisbenzoate[5,7] with identical vertices, have been extensively utilized for the construction of porous MOFs. However, the utilization of asymmetrical aromatic polycarboxylates for MOF synthesis has been less well investigated.[8] In order to enrich the library of organic linkers, some new strategies have been developed. One of these strategies is to reduce the symmetry by systematic and symmetrical extension of organic linkers (Scheme 1). Matzger et al. reported how the organic linkers can be tuned by the reduction of linker symmetry.[8a,e] Although the method is beneficial for the suppression of framework interpenetration, the frameworks constructed by larger organic linkers show a tendency to collapse when the guest is removed.

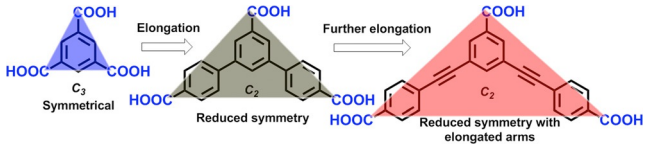

Scheme 1. Elongated tricarboxylate organic linkers.

Herein, we report a new asymmetrical tricarboxylate (**H_3L**) as an organic linker, which was synthesized by a strategy of symmetry-reduced extension. Under solvothermal conditions, the organic linker **H_3L** reacts with copper(II) nitrate to form a twofold interpenetrated porous MOF (**1**) with a Pt_3O_4 topological structure. Despite the structural interpenetration, the activated form of this MOF is highly porous, showing a high selectivity for CO_2 uptake over CH_4 and N_2 and also a significant H_2 uptake capability.

Results and Discussion

The organic linker **H_3L** was prepared by a palladium-catalyzed Sonogashira coupling between dialkyne and methyl 4-iodobenzoate, followed by base-catalyzed hydrolysis (Scheme 2). The solvothermal reaction between **H_3L** and copper(II) nitrate in DMF/HNO_3 (4.0/0.6, v/v) mixed solution (DMF = *N*,*N*′-dimethylformamide) at 70 °C for 2 d afforded blue block-like crystals. Single-crystal X-ray diffraction analysis reveals that **1** crystallizes in the *I*4/*m* space group with a tetragonal crystal system (Table 1). The unit cell of **1** consists of two types of paddle-wheel $Cu_2(COO)_4$ secondary building units (SBUs), which are interconnected by L^{3-} in order to make the twofold interpenetrated three-dimensional (3D) network. One type of paddle-wheel has two *p*-benzoate and two *m*-benzoate groups from

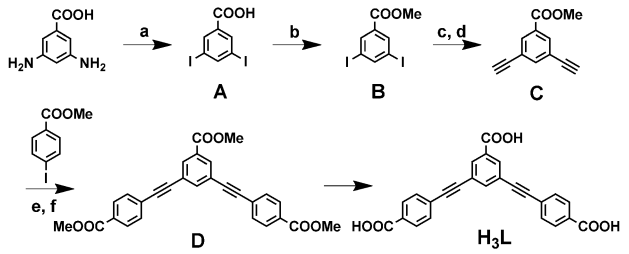

Scheme 2. Synthetic route to linker $\mathbf{H_3L}$: a) 1. $NaNO_2/H_2SO_4$, 2. KI; b) $(MeO)_2SO_2$, K_2CO_3, acetone; c) trimethylsilylacetylene (TMSA), $[PdCl_2(PPh_3)_2]$, CuI, *N*,*N*′-diisopropylethylamine (DIPEA), THF; d) *n*-tetrabutylammonium fluoride (TBAF), THF; e) $[PdCl_2(PPh_3)_2]$, CuI, DIPEA, THF; f) KOH, MeOH/THF, HCl.

Table 1. Crystallographic data and structural refinement summary of **1**.

	1
Molecular formula	$C_{50}H_{22}Cu_3O_{15}$
Formula weight	1053.29
T (K)	103(2)
Wavelength (Å)	0.71073
Crystal system	tetragonal
Space group	*I*4/*m*
Unit cell dimensions	$a = 31.369(4)$ Å, $c = 19.806(3)$ Å, $\alpha = \beta = \gamma = 90°$
V (Å^3)	19489(6)
Z	4
D_{calc} (g cm^{-3})	0.359
F (000)	2116
Crystal size (mm)	0.240×0.200×0.200
θ range (°)	1.779 to 25.838°
Reflections collected/ unique/ parameters	9606/3671/317
R_1/wR_2	0.0874/0.2978
GOF on F^2	1.059

four different $\mathbf{L}^{3-}$ units, whereas another $Cu_2(COO)_4$ paddlewheel consists of only *p*-benzoate moieties. In the unit cell, the ratio of the two types of paddlewheels is 2:1 in order to satisfy the overall stoichiometry of $\mathbf{L}^{3-}$ (Figure 1a and Figure S1 in the Supporting Information). One type of cage was observed in the framework. Each cage is surrounded by six $Cu_2(COO)_4$ paddlewheel motifs for the construction of an octahedron building unit (Figure 1b). Eventually, these cage motifs are interpenetrated in nature, leaving porous channels with the diameter about 13.8 Å along the *c*-axis (Figure S1 in the Supporting Information). The binuclear paddlewheel copper cluster connected with four $\mathbf{L}^{3-}$ units can be considered as a 4-connected node, and each $\mathbf{L}^{3-}$ unit joint with three paddlewheel copper clusters to form a 3-connected node.

To better understand such a complicated structure, the topology of **1** was studied by Topos 4.0 software.[9] The network topology is based on 4-connected Cu paddlewheel clusters and 3-connected ligands. The structure has a 3,4-connected (3,4-c) net with stoichiometry $(3\text{-c})_4(4\text{-c})_3$. Therefore, it self-assembles into a three-dimensional net with the point Schläfli symbol of $\{8^3\}_4\{8^6\}_3$, which is Pt_3O_4 topology based on the Reticular Chemistry Structure Resource (RCSR) database (Figure 1c,d).[10] Total potential solvent-accessible volume calculated by PALTON was 12389 Å^3, which corresponds to 63.6% of the unit cell volume. Thermogravimetric analysis (TGA) was performed to examine the framework stability. The TGA curve indicates that **1** is thermally stable up to 300 °C (Figure S2 in the Supporting Information).

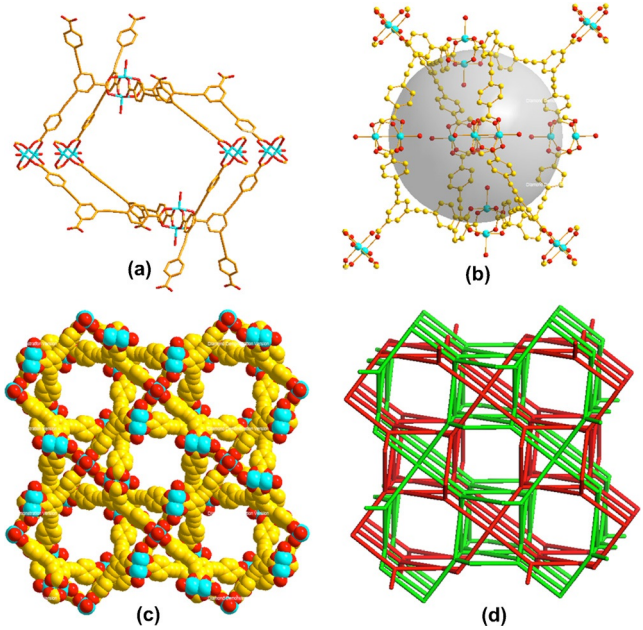

Figure 1. Crystal view of **1**: a) coordination environment of metal ions and ligands in **1**, b) molecular cage, c) twofold interpenetrated Pt_3O_4 framework topology, and d) space-filling model of the interpenetrated microporous framework **1** along the *c*-axis: Cu aqua; C yellow; O red. Hydrogen atoms were omitted for clarity.

Achieving permanent porosity upon the removal of solvent guest molecules from the interpenetrated network is a challenging task. In some cases, the network collapses upon the activation. Matzger et al. reported a copper-paddlewheel-connected MOF, UMCM-151, using an unsymmetrical tritopic organic linker that is shorter than $\mathbf{H_3L}$ (Scheme 1).[8e] The single-crystal structure of UMCM-151 revealed a non-interpenetrated porous network with 30 Å oblong-shaped channels along the *c*-axis. In spite of having a non-interpenetrated porous network, UMCM-151 collapsed upon activation and cannot be utilized for any further applications.[8e] The collapse of the network may be attributed to insufficient junction points offered by the coordination of three carboxylate groups with Cu^{II} paddlewheels in a stable conformation. In contrast, **1** with a twofold interpenetrating network shows high stability and porosity even after the removal of solvent guest molecules. The permanent porosity of activated **1** was confirmed by a N_2 sorption isotherm recorded at 77 K, which displayed a reversible type I isotherm. The measured Brunauer–Emmett–Teller (BET) surface area is 2297 m^2 g^{-1} with a pore volume of 0.845 cm^3 g^{-1} (Figure 2a and Figure S3 in the Supporting Information). The calculated pore width is about 14 Å, which is in good agreement with the value observed in crystallographic measurements (Figure 2a and Figure S1 in the Supporting Information). Although this BET value is lower than that of some isoreticular MOFs,[11]

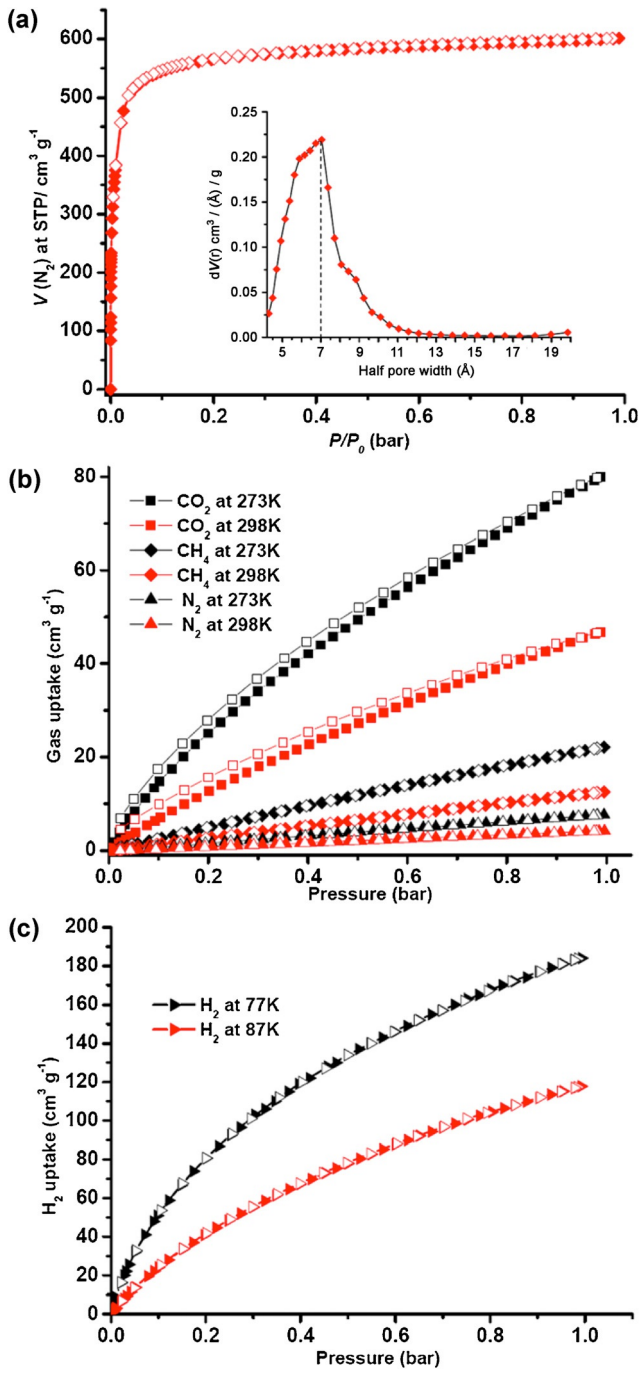

Figure 2. Gas sorption isotherms of activated **1** for a) N_2 at 77 K (inset shows the pore-width distribution curve), b) CO_2, CH_4, and N_2 at 273 K and 298 K, and c) H_2 at 77 K and 87 K. Filled symbols denote adsorption, and empty symbols denote desorption.

for example, NOTT-102 (2942 $m^2 g^{-1}$)[11c] and NOTT-103 (2929 $m^2 g^{-1}$),[11c] it is surprisingly higher than that of some of highly porous non-interpenetrated MOFs, for example, PCN-11 (1931 $m^2 g^{-1}$),[11b] NOTT-106 (1855 $m^2 g^{-1}$),[11c] NOTT-107 (1822 $m^2 g^{-1}$),[11c] PCN-16′ (1760 $m^2 g^{-1}$),[11d] PCN-14 (1753 $m^2 g^{-1}$),[11a] NOTT-109 (1718 $m^2 g^{-1}$),[11c] NOTT-100 (1661 $m^2 g^{-1}$),[11c] UTSA-40 (1630 $m^2 g^{-1}$),[11e] and PCN-10 (1407 $m^2 g^{-1}$).[11b] In addition, **1** is also comparable to certain non-interpenetrated porous MOFs,[12] namely, NOTT-105 (2387 $m^2 g^{-1}$),[11c] HNUST-2 (2366 $m^2 g^{-1}$),[12b] NOTT-101 (2316 $m^2 g^{-1}$),[11c] and SNU-50 (2300 $m^2 g^{-1}$).[12a] To the best of our knowledge, **1** possesses the highest BET surface area among the reported interpenetrated MOFs (Table 2).

Table 2. Comparison of some microporous interpenetrated and non-interpenetrated MOFs in terms of the surface area and pore volume.

Materials	S_{BET} [$m^2 g^{-1}$]	Pore volume V_p[a] [$cm^3 g^{-1}$]
	Interpenetrated MOFs	
1	2297	0.845
JUC-100[13]	2081	0.808
PCN-124[14]	2002	0.579
$[Cu_{24}(\mathbf{L})_{12}(H_2O)_{12}]$[15]	1879	–
α-$[Zn_4O(\mathbf{L1})_3]$[16]	1790	–
$[Co_4O(\mathbf{L})_3]$[17]	1355	0.700
PMOF-3 (1 a and 1 b)[18]	1200, 1840	–
SUMOF-2,3,4[19]	1167, 1163, 1612	0.421, 0.448, 0.580
HNUST-4[20]	1136	0.458
UTSA-38[21]	1060	0.610
mIm-MOF-14[22]	1011	–
	Non-interpenetrated MOFs	
PCN-11[11b]	1931	0.910
NOTT-107[11c]	1822	0.767
PCN-16′[11d]	1760	0.840
PCN-14[11a]	1753	0.870
NOTT-109[11c]	1718	0.850
NOTT-100[11c]	1661	0.677
UTSA-40[11e]	1630	0.650
PCN-10[11b]	1407	0.670

The high surface area, unsaturated metal sites, and alkyne functionalities in the framework of activated **1** encouraged us to explore its gas-uptake capability. As a result, we measured low-pressure CO_2, CH_4, N_2, and H_2 sorption isotherms of activated **1** at different temperatures (Figure 2 b,c and Table S1 in the Supporting Information). The CO_2 adsorption isotherm indicates a relatively high CO_2 uptake of 79.9 $cm^3 g^{-1}$ (15.7 wt%) and 46.8 $cm^3 g^{-1}$ (9.2 wt%) under 1 bar at 273 K and 298 K, respectively (Figure 2 b). This relatively high uptake may be attributed to the involvement of unsaturated metal sites and tetracarboxylate units. The CO_2 uptake value is relatively lower than some of the reported interpenetrated MOFs, for example, PCN-124 (204.0 $cm^3 g^{-1}$ at 273 K and 1 bar)[14] and HNUST-4 (100.9 $cm^3 g^{-1}$ at 273 K and 1 bar),[20] and is comparable to the CO_2 uptake values some other reported interpenetrated MOFs, for example, MOF-1 (63.5 $cm^3 g^{-1}$ at 298 K and 1 bar)[15] and SUMOF-2, SUMOF-3, and SUMOF-4 (95.4, 77.1, and 80.6 $cm^3 g^{-1}$ at 273 K and 1 bar).[19] Interestingly, the CO_2 uptake capacity of **1** is comparable to that of some of the best-performing ZIF materials (Table 3), for example, ZIF-20 (69.8 $cm^3 g^{-1}$ at 273 K and 1 bar),[23] ZIF-68 (37.6 $cm^3 g^{-1}$ at 298 K and 1 bar),[24] ZIF-69 (40.6 $cm^3 g^{-1}$ at 298 K and 1 bar),[24] ZIF-70 (55.0 $cm^3 g^{-1}$ at 298 K and 1 bar),[24] ZIF-78 (51.5 $cm^3 g^{-1}$ at 298 K and 1 bar),[24] ZIF-79 (33.5 $cm^3 g^{-1}$ at 298 K and 1 bar),[24] ZIF-81 (38.2 $cm^3 g^{-1}$ at 298 K and 1 bar),[24] and ZIF-82 (52.7 $cm^3 g^{-1}$ at 298 K and 1 bar).[24] We also compared the uptake capacity of **1** with that

Table 3. Comparison of some microporous interpenetrated and non-interpenetrated MOFs in terms of their CO_2 uptake capacity.

Materials	Surface area [$m^2 g^{-1}$]	CO_2 uptake at 1 bar [$cm^3 g^{-1}$] 273 K	298 K	CO_2 Qst [$kJ mol^{-1}$]
	Interpenetrated MOFs			
1	2297	79.9	46.8	25.5
JUC-100[13]	2081	–	–	–
PCN-124[14]	2002	204.0	114.0 (295 K)	26.0
$[Cu_{24}(\mathbf{L})_{12}(H_2O)_{12}]$[15]	1879	–	63.5	–
SUMOF-2,3,4[19]	1167, 1163, 1612	95.4, 77.1, 80.6	–	–
$[Co_4O(L)_3]$[17]	1355	76.6	–	–
HNUST-4[20]	1136	100.9	62.9	27.2
$Zn_4O(2,6\text{-}NDC)_3\text{-}(DMF)_{1.5}(H_2O)_{0.5}$ (or UTSA-38)[21]	1060	76.0	39.0 (295 K)	28.1
YO-MOF[25]	340 (CO_2 isotherm)	80 (hysteresis)	–	–
$C_{16}H_{10}CuN_4O_4$ (or $[Cu(\mathbf{HL})_2]$)[26]	550	124 (30 bar)	93 (30 bar)	17.5
MMCF-1[27]	500	66.7	45.8	~26.0
$[Zn_3L_2(btc)_2(H_2O)]\cdot$(guest),	239	46.0	–	–
$[CdL(bdc)]\cdot$(guest)[28]	31 (type II)	–	–	–
$\{[Cd_2(TPPBDA)(OBA)_2]\cdot 4DMA\cdot 8H_2O\}_n$[29]	–	33.0	14.0	23–25
CAU-5[30]	554 (N_2) 805 (Ar)	–	50.0	–
$[Cu_2L_2(H_2O)_2]Na_2(Me_2NH_2)_4\text{-}[Cd_7L_{10}]\cdot 9H_2O\cdot 17Me_2NH\cdot 2DMF$[31]	132.7	–	25.9	–
$[Zn_4O(\mathbf{1})_3]$[32]	131	–	–	–
$\alpha\text{-}[Zn_4O(\mathbf{L1})_3]$[16]	1790	–	–	–
mIm-MOF-14[22]	1011	–	–	24.0
$\{Zn_4O[Cu(L)_2]_2\}$[33]	1300 (calculated)	–	–	–
ZJU-30[34]	228	–	–	–
interpenetrated MOF-5[35]	1130 (Langmuir)	–	–	–
$Zn_2(BBA)_2(CuPyen)\cdot G_x$ (or M′MOF-20)[36]	62.0	17.5	10.0 (295 K)	28.4
$Zn_{1.5}[L\text{-}13\text{-}](H_2O)$ (or B-MOF-1)[37]	368 (87 K) 406 (77 K)	27.0	–	–
$[Co(pybz)_2]$[38]	765.2 (Langmuir) 260.5 (Langmuir)	133 (195 K) 44 (195 K)	–	–
$Zr_6(\mu3\text{-}O)_4(\mu_3\text{-}OH)_4(OH)_6\text{-}(H_2O)_6(BTB)_2\cdot 6DMF\cdot H_2O$[39]	613	–	–	–
$Zn_4O(RCO_2)_6$ SBU[40]	≈580 (Langmuir)	–	–	–
	Non-interpenetrated MOFs			
ZIF-20[23]	800 (Langmuir)	70.0	–	–
ZIF-68[24]	1090	–	37.6	–
ZIF-69[24]	950	–	40.6	–
ZIF-70[24]	1730	–	55.0	–
ZIF-78[24]	620	–	51.5	–
ZIF-79[24]	810	–	33.5	–
ZIF-81[24]	760	–	38.2	–
ZIF-82[24]	1300	–	52.7	–

of other reported interpenetrated MOFs (Table 3). The low CH_4 (21.9 and 12.5 $cm^3 g^{-1}$ at 273 K and 1 bar as well as 298 K and 1 bar, respectively) and N_2 (7.6 and 4.2 $cm^3 g^{-1}$ at 273 K and 1 bar as well as 298 K and 1 bar, respectively) uptake capacities indicate that **1** selectively adsorbs CO_2 over N_2 and CH_4. Based on the initial slope of the adsorption isotherm, the measured selective separation ratios of CO_2/N_2 for **1** are 21.6 and 18.2 at 273 K and 298 K, respectively (Figure 3). The values for CO_2/CH_4 are 6.9 and 5.6 at 273 K and 298 K, respectively (Figure S4 in the Supporting Information). The isosteric heats (Q_{st}) of CO_2 and CH_4 adsorption at zero surface coverage are 25.5 and 21.3 $kJ mol^{-1}$, respectively. The values decreased slowly with increased loading (Figures S5 and S6 in the Supporting Information).

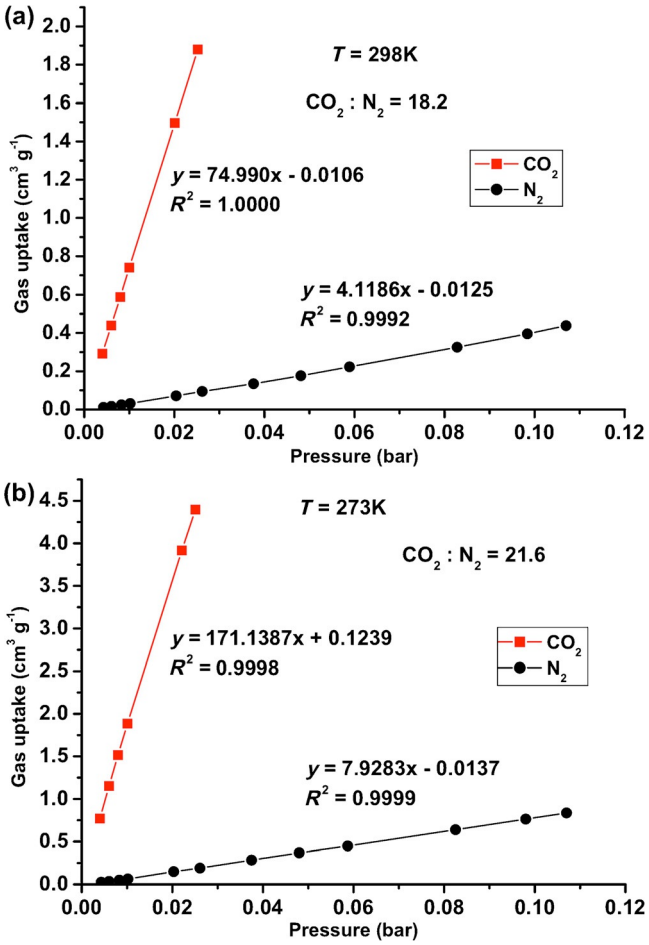

Figure 3. Initial slope calculation of CO_2 and N_2 isotherms for **1** at a) 273 K and b) 298 K.

The interpenetrated network of activated **1** shows significant H_2 uptake as well, that is, 1.64 and 1.05 wt% (184.3 and 117.8 $cm^3 g^{-1}$) at 77 K and 87 K under 1 bar, respectively (Figure 2c). These values are higher than those of some well-known MOFs, for example, PCN-9 (1.53 wt%),[41] HNUST-4 (1.52 wt%),[20] NOTT-119 (1.40 wt%),[42] IRMOF-2 (1.21 wt%),[43] IRMOF-6 (1.48 wt%),[43] IRMOF-8 (1.45 wt%),[44] HNUST-1 (1.44 wt%),[45] IRMOF-3 (1.42 wt%),[43] PCN-6′ (1.37 wt%),[46] IRMOF-20 (1.35 wt%),[43] MOF-177 (1.25 wt%),[47] IRMOF-9 (1.15 wt%),[43] and MOF-508 (0.80 wt%)[48] at 77 K and 1 bar. The calculated isosteric heat of H_2 adsorption at zero coverage

is 6.30 kJ mol^{-1} (Figure S7 in the Supporting Information). This value is in close agreement with that of most MOFs having exposed metal sites.[1e] The powder X-ray diffraction pattern of a bulk crystalline sample of **1** after the gas adsorption experiments was identical to the simulated pattern and the diffraction pattern of pristine **1** (Figure S8 in the Supporting Information), further supporting the high stability and permanent porosity of the network.

Conclusion

In summary, we have rationally designed and synthesized an asymmetrical tricarboxylate organic linker with elongated arms for the construction of a new twofold interpenetrated microporous MOF with a Pt_3O_4 topology. Upon activation, **1** shows the highest BET surface area (2297 m^{2}g^{-1}) among all the reported interpenetrated MOFs. Interestingly, the value is comparable and even higher than that of some well-known highly porous non-interpenetrated MOFs. Despite its interpenetrated framework, the activated **1** presents high CO_2 and H_2 uptake capability, providing high CO_2/N_2 and CO_2/CH_4 selectivity at ambient conditions. Thus, the high selectivity of **1** for CO_2 over N_2 and CH_4 makes it promising for potential gas-separation and -storage applications.

Experimental Section

Materials and methods: Copper nitrate trihydrate, 3,5-diaminobenzoic acid, dimethyl sulfate, potassium iodide, sodium nitrite, and trimethylsilylacetylene were purchased from Sigma–Aldrich and were used as received. Methyl 4-iodobenzoate was purchased from TCI chemicals. Dichloromethane (DCM) was freshly distilled from calcium hydride. NMR spectra were recorded on either a Bruker AV 300 or a Bruker AV400 at room temperature. Electrospray ionization mass spectrometry (ESI-MS) experiments were carried out on a ThermoFinnigan LCQ Fleet MS. Thermogravimetric analysis (TGA) was carried out on a TGA-Q500 thermoanalyzer with a heating rate of 5 °C min^{-1} under nitrogen atmosphere. Powder X-ray diffraction measurements were performed on a Bruker D8 diffractometer using Cu-Kα radiation (λ = 1.5418 Å) at room temperature.

Synthesis of A: Compound **A** was synthesized by a modified literature procedure.[49] A 1 L three-neck round-bottom flask equipped with a mechanical stirrer and a thermometer was charged with 3,5-diaminobenzoic acid (6.00 g, 39.40 mmol) and 25% H_2SO_4 solution (70 mL). The reaction mixture was cooled to −5 °C with an ice-salt bath. Then, the temperature of the reaction mixture was carefully monitored. To this cooled reaction mixture, an ice-cooled solution of $NaNO_2$ (6.53 g, 394 mmol, 10 mL) was added dropwise. After the solution had been stirred at −5 °C for 1 h, urea (497 mg, 8.30 mmol) was added to get rid of excess $NaNO_2$. Then, an aqueous solution of potassium iodide (65.50 g, 394 mmol) was added dropwise, and the reaction mixture was stirred at −5 °C for an additional 2.5 h. It was heated to 60 °C for 30 min. After cooling down to room temperature, the reaction mixture was filtered. The precipitate was dissolved in diethyl ether and the organic layer was washed with $Na_2S_2O_3$ (3×) to remove iodine. The organic layer was dried over anhydrous Na_2SO_4 and the solvent was removed by evaporation. The crude product was purified by chromatography on silica gel using EtOAc/CH_2Cl_2 (5:95 to 20:80, v/v) as the eluent to afford 3,5-diiodobenzoic acid (**A**) as a yellowish white solid (yield 60%). ^{1}H NMR (300 MHz, [D$_6$]DMSO): δ = 13.49 (s, 1 H, COOH), 8.35 (s, 1 H, 2,6-H), 8.21 ppm (s, 2 H, 4-H); ^{13}C NMR ([D$_6$]DMSO, 75 MHz): δ = 165.12, 148.66, 137.45, 134.78, 96.60 ppm; HRMS (ESI-TOF) *m/z* calcd for $C_7H_4I_2O_2$ [*M*+H]$^+$: 374.8379, found 374.8376.

Synthesis of B: A suspension of 3,5-diiodobenzoic acid (**A**) (1.00 g, 2.67 mmol), K_2CO_3 (437 mg), and dimethyl sulfate (0.27 mL) in anhydrous acetone (25 mL) was refluxed at 56 °C for 12 h. After the reaction mixture had cooled down to room temperature, water (5 mL) was added. The mixture was stirred under ambient conditions for 12 h. The solvent was removed by evaporation. The residue was dissolved in CH_2Cl_2 and the organic layer was washed with water three times. Finally, the organic layer was dried over anhydrous Na_2SO_4, and the volatiles were removed by evaportation leaving a crude solid. The solid was then purified on silica gel using hexane as the eluent to afford compound **B** as a white solid (yield 95%). ^{1}H NMR (300 MHz, [D$_6$]DMSO): δ = 8.38 (s, 1 H, 4-H), 8.20 (s, 2 H, 2,6-H), 3.86 ppm(s, 3 H, OCH_3); ^{13}C NMR ([D$_6$]DMSO, 100 MHz): δ = 164.11, 149.10, 137.07, 133.42, 96.76, 53.19 ppm; HRMS (ESI-TOF) *m/z* calcd for $C_8H_7I_2O_2$ [*M*+H]$^+$: 388.8536, found 388.8554.

Synthesis of C: A mixture of compound **B** (2.00 g, 5.17 mmol), trimethylsilylacetylene (2.19 mL, 15.51 mmol), [Pd(PPh_3)$_2$Cl$_2$] (181 mg, 0.25 mmol), and CuI (99 mg, 0.50 mmol) in diisopropylethyl amine (DIPEA, 30 mL) and THF (30 mL) was heated at 60 °C under nitrogen for 12 h and then cooled to room temperature. The mixture was filtered and the solvent was removed by evaporation. The crude product was deprotected without further purification.

In a 100 mL round-bottom flask, the trimethylsilylated compound (1 g) was dissolved in a mixture of THF (20 mL) and methanol (10 mL). To this reaction mixture, tetrabutylammonium fluoride (TBAF) solution (1 M in THF, 2 mL) was added. The mixture was stirred undert ambient conditions for 2 h. The solvent was removed by evaporation, and the desilylated crude product was purified by column chromatography (silica gel, ethyl acetate/hexane 10–30% v/v). The pure product was obtained as brownish white solid (yield 72%). ^{1}H NMR (300 MHz, $CDCl_3$): δ = 8.10 (s, 2 H, 2,6-H), 7.75 (s, 1 H, 4-H), 3.92 (s, 3 H, OCH_3), 3.13 ppm (s, 2 H, ethynyl-H); ^{13}C NMR ($CDCl_3$, 100 MHz): δ = 165.47, 139.32, 133.26, 130.84, 123.03, 81.59, 78.90, 52.51 ppm; HRMS (ESI-TOF) *m/z* calcd for $C_{12}H_9O_2$ [*M*+H]$^+$: 185.0603, found 185.0582.

Synthesis of D: A mixture of compound **C** (0.58 g, 3.15 mmol), methyl 4-iodobenzoate (1.78 g, 6.78 mmol), [Pd(PPh_3)$_2$Cl$_2$] (166 mg, 0.24 mmol), and CuI (92 mg, 0.48 mmol) in DIPEA (15 mL) and THF (15 mL) was stirred at room temperature under nitrogen atmosphere for 24 h. The mixture was filtered and the filtrate was evaporated to dryness. The residue was purified by column chromatography on silica gel using CH_2Cl_2 as the eluent. The pure compound **D** was isolated as a yellowish white solid (yield 70%). ^{1}H NMR (300 MHz, $CDCl_3$): δ = 8.19 (s, 2 H), 8.05 (d, 4 H, *J* = 8.2 Hz), 7.89 (s, 1 H), 7.60 (d, 4 H, *J* = 8.3 Hz), 3.97 (s, 3 H, OCH_3), 3.94 ppm (s, 6 H, OCH_3); ^{13}C NMR ($CDCl_3$, 100 MHz): δ = 166.44, 165.58, 138.35, 132.67, 131.65, 131.04, 130.01, 129.61, 127.20, 123.76, 90.20, 90.18, 52.55, 52.29 pm; HRMS (ESI) *m/z*: [*M*+H]$^+$ calcd for $C_{28}H_{21}O_6$, 453.1338; found, 453.1326.

Synthesis of H_3L: A mixture of compound **D** (400 mg, 0.88 mmol), NaOH (500 mg, 12.50 mmol), THF (20 mL), and water (5 mL) was stirred at ambient temperature for 12 h. The mixture was then concentrated under reduced pressure. The concentrated reaction mixture was acidified with cold 3 M HCl in an ice bath. The white precipitate that appeared was filtered and washed with plenty of dis-

tilled water. The precipitate was then dried under reduced pressure in order to get pure **H_3L** as a white solid (yield 90%). ^{1}H NMR (300 MHz, [D$_6$]DMSO): $\delta = 13.31$ (s, 3H), 8.11 (s, 2H), 8.05 (s, 1H), 8.00 (d, 4H, $J = 8.3$ Hz), 7.73 ppm (d, 4H, $J = 8.2$ Hz); ^{13}C NMR ([D$_6$]DMSO, 100 MHz): $\delta = 167.27$, 166.51, 137.41, 134.71, 132.85, 132.16, 132.00, 130.02, 126.29, 123.31, 90.47, 90.43 ppm; HRMS (ESI) m/z: $[M+H]^+$ calcd for $C_{25}H_{15}O_6$, 411.0869; found, 411.0874.

Synthesis of 1: A mixture of **H_3L** (10.0 mg, 0.024 mmol) and $Cu(NO_3)_2 \cdot 3H_2O$ (23.2 mg, 0.096 mmol) was dissolved in DMF (4 mL) in a 10 mL screw-capped vial. To this solution, HNO_3 (0.6 mL) was added, and the vial was tightly capped and placed in an oven at 70 °C for 3 days. The obtained block-like blue crystals were washed twice with DMF and dried in air to afford **1** (yield ≈ 60% based on **H_3L**). IR (KBr): $\tilde{\nu} = 1658$, 1602, 1398, 1257, 1176, 1101, 1016, 862, 781, 738, 698, 665 cm^{-1}.

X-ray crystallography: A suitable single crystal was selected for single-crystal X-ray diffraction analysis. Crystallographic data were collected on an Agilent SuperNova diffractometer with an Atlas CCD equipped with Mo-Kα radiation ($\lambda = 0.71073$ Å) at 103 K. The single crystal of **1** for X-ray diffraction analyses was mounted onto a glass fiber. The program SAINT was used for integration of the diffraction profiles,[11e] and the data were corrected for absorption by using the SADABS program.[23] The structure was solved by direct methods using the SHELXS program of the SHELXTL package and refined by full-matrix least-squares analyses on F^2 (SHELXTL-97).[24] Metal atoms in each complex were located from the E-maps, and other non-hydrogen atoms were located in successive difference Fourier syntheses. The hydrogen atoms of the ligands were generated theoretically onto the specific atoms and refined isotropically with fixed thermal factors. The solvent molecules were highly disordered and cannot be modeled, thus the SQUEEZE routine of PLATON was used to remove the contributions of the solvent molecules to the scattering.[25] Further details of crystallographic data and structural analyses for **1** are summarized in Table 1. CCDC 1033100 contains the supplementary crystallographic data for **1**. These data can be obtained free of charge from The Cambridge Crystallographic Data Centre via www.ccdc.cam.ac.uk/data_request/cif.

Gas adsorption studies: Low-pressure gas sorption measurements were performed by using Quantachrome Instruments AutosorbiQ (Boynton Beach, Florida USA) with extra-high-purity gases. The nonvolatile solvents were exchanged by soaking the MOF crystals in CH_2Cl_2 for 3 days, during which CH_2Cl_2 was replaced three times each day. Then, the sample was placed into a sample cell and dried for 8 h under vacuum at 90 °C by using the "outgasser" function before the measurements. The BET surface area, total pore volume, and pore size distribution were calculated from the N_2 sorption isotherms at 77 K. The pore size distribution was calculated based on the Non-Local Density Functional Theory (NL-DFT, a zeolite/silica model containing spherical/cylindrical pores) model in the Quantachrome ASiQwin 2.01 software package. The isosteric heats of adsorption (Q_{st}) for CO_2, CH_4, and H_2, defined by the Clausius–Claperyon equation [Eq. (1)],

$$Q_{st} = RT^2 \left(\frac{\partial \ln p}{\partial T} \right)_q \quad (1)$$

were determined by using the CO_2 and CH_4 adsorption isotherms at 273 and 298 K, respectively, and the H_2 adsorption isotherms at 77 and 87 K.

Acknowledgements

*This work was supported by the National Research Foundation (NRF), Prime Minister's Office, Singapore under its NRF Fellowship (NRF2009NRF-RF001-015) and Campus for Research Excellence and Technological Enterprise (CREATE) Programme-Singapore Peking University Research Centre for a Sustainable Low-Carbon Future, as well as the NTU-A*Star Silicon Technologies Centre of Excellence under the program grant No. 1123510003.*

Keywords: gas adsorption · metal–organic frameworks · porous materials

[1] a) J.-R. Li, R. J. Kuppler, H.-C. Zhou, *Chem. Soc. Rev.* **2009**, *38*, 1477–1504; b) L. J. Murray, M. Dinca, J. R. Long, *Chem. Soc. Rev.* **2009**, *38*, 1294–1314; c) A. Phan, C. J. Doonan, F. J. Uribe-Romo, C. B. Knobler, M. O'Keeffe, O. M. Yaghi, *Acc. Chem. Res.* **2010**, *43*, 58–67; d) J.-R. Li, Y. Ma, M. C. McCarthy, J. Sculley, J. Yu, H.-K. Jeong, P. B. Balbuena, H.-C. Zhou, *Coord. Chem. Rev.* **2011**, *255*, 1791–1823; e) M. P. Suh, H. J. Park, T. K. Prasad, D.-W. Lim, *Chem. Rev.* **2012**, *112*, 782–835; f) K. Sumida, D. L. Rogow, J. A. Mason, T. M. McDonald, E. D. Bloch, Z. R. Herm, T.-H. Bae, J. R. Long, *Chem. Rev.* **2012**, *112*, 724–781; g) J. Liu, P. K. Thallapally, B. P. McGrail, D. R. Brown, J. Liu, *Chem. Soc. Rev.* **2012**, *41*, 2308–2322; h) Y. He, W. Zhou, G. Qian, B. Chen, *Chem. Soc. Rev.* **2014**, *43*, 5657–5678; i) B. Van de Voorde, B. Bueken, J. Denayer, D. De Vos, *Chem. Soc. Rev.* **2014**, *43*, 5766–5788.

[2] a) J. Lee, O. K. Farha, J. Roberts, K. A. Scheidt, S. T. Nguyen, J. T. Hupp, *Chem. Soc. Rev.* **2009**, *38*, 1450–1459; b) L. Ma, C. Abney, W. Lin, *Chem. Soc. Rev.* **2009**, *38*, 1248–1256; c) T. Uemura, N. Yanai, S. Kitagawa, *Chem. Soc. Rev.* **2009**, *38*, 1228–1236; d) A. Corma, H. García, F. X. Llabrés i Xamena, *Chem. Rev.* **2010**, *110*, 4606–4655; e) M. Yoon, R. Srirambalaji, K. Kim, *Chem. Rev.* **2012**, *112*, 1196–1231; f) J. Liu, L. Chen, H. Cui, J. Zhang, L. Zhang, C.-Y. Su, *Chem. Soc. Rev.* **2014**, *43*, 6011–6061.

[3] a) B. Li, W. Gu, L.-Z. Zhang, J. Qu, Z.-P. Ma, X. Liu, D.-Z. Liao, *Inorg. Chem.* **2006**, *45*, 10425–10427; b) M. Yuan, F. Zhao, W. Zhang, Z.-M. Wang, S. Gao, *Inorg. Chem.* **2007**, *46*, 11235–11242.

[4] a) S. Kitagawa, R. Kitaura, S.-i. Noro, *Angew. Chem. Int. Ed.* **2004**, *43*, 2334–2375; *Angew. Chem.* **2004**, *116*, 2388–2430; b) C. Seward, W.-L. Jia, R.-Y. Wang, G. D. Enright, S. Wang, *Angew. Chem. Int. Ed.* **2004**, *43*, 2933–2936; *Angew. Chem.* **2004**, *116*, 2993–2996; c) Z. Xie, L. Ma, K. E. deKrafft, A. Jin, W. Lin, *J. Am. Chem. Soc.* **2010**, *132*, 922–923; d) Y. Cui, Y. Yue, G. Qian, B. Chen, *Chem. Rev.* **2012**, *112*, 1126–1162.

[5] W. Lu, Z. Wei, Z.-Y. Gu, T.-F. Liu, J. Park, J. Park, J. Tian, M. Zhang, Q. Zhang, T. Gentle III, M. Bosch, H.-C. Zhou, *Chem. Soc. Rev.* **2014**, *43*, 5561–5593.

[6] S. S.-Y. Chui, S. M.-F. Lo, J. P. H. Charmant, A. G. Orpen, I. D. Williams, *Science* **1999**, *283*, 1148–1150.

[7] a) B. Chen, M. Eddaoudi, S. T. Hyde, M. O'Keeffe, O. M. Yaghi, *Science* **2001**, *291*, 1021–1023; b) T. Devic, C. Serre, N. Audebrand, J. Marrot, G. Férey, *J. Am. Chem. Soc.* **2005**, *127*, 12788–12789; c) P. V. Dau, K. K. Tanabe, S. M. Cohen, *Chem. Commun.* **2012**, *48*, 9370–9372; d) H. Furukawa, K. E. Cordova, M. O'Keeffe, O. M. Yaghi, *Science* **2013**, *341*, 1230444.

[8] a) A. G. Wong-Foy, O. Lebel, A. J. Matzger, *J. Am. Chem. Soc.* **2007**, *129*, 15740–15741; b) H.-T. Chung, H.-L. Tsai, E.-C. Yang, P.-H. Chien, C.-C. Peng, Y.-C. Huang, Y.-H. Liu, *Eur. J. Inorg. Chem.* **2009**, 3661–3666; c) K.-L. Huang, X. Liu, X. Chen, D.-Q. Wang, *Cryst. Growth Des.* **2009**, *9*, 1646–1650; d) C.-S. Lim, J. K. Schnobrich, A. G. Wong-Foy, A. J. Matzger, *Inorg. Chem.* **2010**, *49*, 5271–5275; e) J. K. Schnobrich, O. Lebel, K. A. Cychosz, A. Dailly, A. G. Wong-Foy, A. J. Matzger, *J. Am. Chem. Soc.* **2010**, *132*, 13941–13948; f) W.-W. He, S.-L. Li, G.-S. Yang, Y.-Q. Lan, Z.-M. Su, Q. Fu, *Chem. Commun.* **2012**, *48*, 10001–10003.

[9] a) S. R. Batten, N. R. Champness, X.-M. Chen, J. Garcia-Martinez, S. Kitagawa, L. Ohrstrom, M. O'Keeffe, M. P. Suh, J. Reedijk, *Pure Appl. Chem.* **2013**, *85*, 1715–1724; b) M. O'Keeffe, M. A. Peskov, S. J. Ramsden, O. M. Yaghi, *Acc. Chem. Res.* **2008**, *41*, 1782–1789.

[10] http://rcsr.net/nets.

[11] a) S. Ma, D. Sun, J. M. Simmons, C. D. Collier, D. Yuan, H.-C. Zhou, *J. Am. Chem. Soc.* **2008**, *130*, 1012 – 1016; b) X.-S. Wang, S. Ma, K. Rauch, J. M. Simmons, D. Yuan, X. Wang, T. Yildirim, W. C. Cole, J. J. López, A. d. Meijere, H.-C. Zhou, *Chem. Mater.* **2008**, *20*, 3145 – 3152; c) X. Lin, I. Telepeni, A. J. Blake, A. Dailly, C. M. Brown, J. M. Simmons, M. Zoppi, G. S. Walker, K. M. Thomas, T. J. Mays, P. Hubberstey, N. R. Champness, M. Schröder, *J. Am. Chem. Soc.* **2009**, *131*, 2159 – 2171; d) D. Sun, S. Ma, J. M. Simmons, J.-R. Li, D. Yuan, H.-C. Zhou, *Chem. Commun.* **2010**, *46*, 1329 – 1331; e) Y. He, S. Xiang, Z. Zhang, S. Xiong, C. Wu, W. Zhou, T. Yildirim, R. Krishna, B. Chen, *J. Mater. Chem. A* **2013**, *1*, 2543 – 2551.
[12] a) T. K. Prasad, D. H. Hong, M. P. Suh, *Chem. Eur. J.* **2010**, *16*, 14043 – 14050; b) Z. Wang, B. Zheng, H. Liu, P. Yi, X. Li, X. Yu, R. Yun, *Dalton Trans.* **2013**, *42*, 11304 – 11311.
[13] J. Jia, F. Sun, Q. Fang, X. Liang, K. Cai, Z. Bian, H. Zhao, L. Gao, G. Zhu, *Chem. Commun.* **2011**, *47*, 9167 – 9169.
[14] J. Park, J.-R. Li, Y.-P. Chen, J. Yu, A. A. Yakovenko, Z. U. Wang, L.-B. Sun, P. B. Balbuena, H.-C. Zhou, *Chem. Commun.* **2012**, *48*, 9995 – 9997.
[15] P. Zhang, B. Li, Y. Zhao, X. Meng, T. Zhang, *Chem. Commun.* **2011**, *47*, 7722 – 7724.
[16] D. Rankine, A. Avellaneda, M. R. Hill, C. J. Doonan, C. J. Sumby, *Chem. Commun.* **2012**, *48*, 10328 – 10330.
[17] E. Quartapelle Procopio, N. M. Padial, N. Masciocchi, S. Galli, J. Enrique Oltra, E. Barea, J. A. R. Navarro, *CrystEngComm* **2013**, *15*, 9352 – 9355.
[18] X. Liu, M. Park, S. Hong, M. Oh, J. W. Yoon, J.-S. Chang, M. S. Lah, *Inorg. Chem.* **2009**, *48*, 11507 – 11509.
[19] Q. Yao, J. Su, O. Cheung, Q. Liu, N. Hedin, X. Zou, *J. Mater. Chem.* **2012**, *22*, 10345 – 10351.
[20] B. Zheng, X. Lin, Z. Wang, R. Yun, Y. Fan, M. Ding, X. Hu, P. Yi, *CrystEngComm* **2014**, *16*, 9586 – 9589.
[21] M. C. Das, H. Xu, Z. Wang, G. Srinivas, W. Zhou, Y.-F. Yue, V. N. Nesterov, G. Qian, B. Chen, *Chem. Commun.* **2011**, *47*, 11715 – 11717.
[22] N. Ko, K. Noh, S. Sung, H. J. Park, S. Y. Park, J. Kim, *Chem. Commun.* **2014**, *50*, 6785 – 6788.
[23] H. Hayashi, A. P. Cote, H. Furukawa, M. O/'Keeffe, O. M. Yaghi, *Nat. Mater.* **2007**, *6*, 501 – 506.
[24] R. Banerjee, H. Furukawa, D. Britt, C. Knobler, M. O'Keeffe, O. M. Yaghi, *J. Am. Chem. Soc.* **2009**, *131*, 3875 – 3877.
[25] K. L. Mulfort, O. K. Farha, C. D. Malliakas, M. G. Kanatzidis, J. T. Hupp, *Chem. Eur. J.* **2010**, *16*, 276 – 281.
[26] C. S. Hawes, R. Babarao, M. R. Hill, K. F. White, B. F. Abrahams, P. E. Kruger, *Chem. Commun.* **2012**, *48*, 11558 – 11560.
[27] W.-Y. Gao, Y. Niu, Y. Chen, L. Wojtas, J. Cai, Y.-S. Chen, S. Ma, *CrystEngComm* **2012**, *14*, 6115 – 6117.
[28] L. Zhou, Y.-S. Xue, Y. Xu, J. Zhang, H.-B. Du, *CrystEngComm* **2013**, *15*, 7315 – 7320.
[29] L. Qin, Z.-M. Ju, Z.-J. Wang, F.-D. Meng, H.-G. Zheng, J.-X. Chen, *Cryst. Growth Des.* **2014**, *14*, 2742 – 2746.
[30] A. Modrow, D. Zargarani, R. Herges, N. Stock, *Dalton Trans.* **2011**, *40*, 4217 – 4222.
[31] R. Luo, H. Xu, H.-X. Gu, X. Wang, Y. Xu, X. Shen, W. Bao, D.-R. Zhu, *CrystEngComm* **2014**, *16*, 784 – 796.
[32] R. K. Deshpande, G. I. N. Waterhouse, G. B. Jameson, S. G. Telfer, *Chem. Commun.* **2012**, *48*, 1574 – 1576.
[33] A. Burgun, R. S. Crees, M. L. Cole, C. J. Doonan, C. J. Sumby, *Chem. Commun.* **2014**, *50*, 11760 – 11763.
[34] J. Cai, J. Yu, H. Xu, Y. He, X. Duan, Y. Cui, C. Wu, B. Chen, G. Qian, *Cryst. Growth Des.* **2013**, *13*, 2094 – 2097.
[35] H. Kim, S. Das, M. G. Kim, D. N. Dybtsev, Y. Kim, K. Kim, *Inorg. Chem.* **2011**, *50*, 3691 – 3696.
[36] Z. Zhang, S. Xiang, K. Hong, M. C. Das, H. D. Arman, M. Garcia, J. U. Mondal, K. M. Thomas, B. Chen, *Inorg. Chem.* **2012**, *51*, 4947 – 4953.
[37] B. A. Blight, R. Guillet-Nicolas, F. Kleitz, R.-Y. Wang, S. Wang, *Inorg. Chem.* **2013**, *52*, 1673 – 1675.
[38] Z. Zhang, S. Xiang, Y.-S. Chen, S. Ma, Y. Lee, T. Phely-Bobin, B. Chen, *Inorg. Chem.* **2010**, *49*, 8444 – 8448.
[39] R. Wang, Z. Wang, Y. Xu, F. Dai, L. Zhang, D. Sun, *Inorg. Chem.* **2014**, *53*, 7086 – 7088.
[40] C. A. Bauer, T. V. Timofeeva, T. B. Settersten, B. D. Patterson, V. H. Liu, B. A. Simmons, M. D. Allendorf, *J. Am. Chem. Soc.* **2007**, *129*, 7136 – 7144.
[41] S. Ma, H.-C. Zhou, *J. Am. Chem. Soc.* **2006**, *128*, 11734 – 11735.
[42] Y. Yan, S. Yang, A. J. Blake, W. Lewis, E. Poirier, S. A. Barnett, N. R. Champness, M. Schroder, *Chem. Commun.* **2011**, *47*, 9995 – 9997.
[43] J. L. C. Rowsell, O. M. Yaghi, *J. Am. Chem. Soc.* **2006**, *128*, 1304 – 1315.
[44] P. Krawiec, M. Kramer, M. Sabo, R. Kunschke, H. Fröde, S. Kaskel, *Adv. Eng. Mater.* **2006**, *8*, 293 – 296.
[45] B. Zheng, H. Liu, Z. Wang, X. Yu, P. Yi, J. Bai, *CrystEngComm* **2013**, *15*, 3517 – 3520.
[46] S. Ma, D. Sun, M. Ambrogio, J. A. Fillinger, S. Parkin, H.-C. Zhou, *J. Am. Chem. Soc.* **2007**, *129*, 1858 – 1859.
[47] J. L. C. Rowsell, A. R. Millward, K. S. Park, O. M. Yaghi, *J. Am. Chem. Soc.* **2004**, *126*, 5666 – 5667.
[48] B. Chen, C. Liang, J. Yang, D. S. Contreras, Y. L. Clancy, E. B. Lobkovsky, O. M. Yaghi, S. Dai, *Angew. Chem. Int. Ed.* **2006**, *45*, 1390 – 1393; *Angew. Chem.* **2006**, *118*, 1418 – 1421.
[49] Y. He, W. Zhou, T. Yildirim, B. Chen, *Energy Environ. Sci.* **2013**, *6*, 2735 – 2744.

Received: March 5, 2015
Published online on June 10, 2015